Bull. Mater. Sci. (2020) 43:136
https://doi.org/10.1007/s12034-020-02121-7

Fabrication of crystalline Sb_2S_3 sheaf structure composed of nanorods by a hot-injection method

LILI LI, LIN YANG*, BOWEN FU and ZHIQIANG LI
College of Physics Science and Technology, Hebei University, Baoding 071002, People's Republic of China
*Author for correspondence (yanglin@hbu.edu.cn)

MS received 4 November 2019; accepted 9 April 2020; published online 10 June 2020

Abstract. Herein, we demonstrate a hot-injection method towards the fabrication of Sb_2S_3. The evolution from amorphous Sb_2S_3 nanoparticles to a sheaf of Sb_2S_3 nanorods cross-linked together occurring with the increase of reaction temperature and time is studied. The structural, compositional and morphological features of Sb_2S_3 products indicate the formation of crystalline Sb_2S_3 with orthorhombic phase and high purity. As the reaction proceeds, it can be observed that the individual nanorod grows along the elongated direction (*c*-axis), and it is noteworthy that its round cross-section could develop into the rectangular cross-section subsequently. In this study we also propose a possible formation mechanism for the growth process of Sb_2S_3, and it reveals that the present hot-injection could provide an ideal growth environment for synthesizing the nanostructured materials by optimizing the experimental parameters.

Keywords. Nanostructures; crystal growth; hot-injection.

1. Introduction

The newly distinct one-dimensional (1-D) nanostructure materials are promising research area, owing to their extraordinary optical, electronic, catalytic and mechanical properties. Sb_2S_3 (stibnite) is a promising semiconductor with abundant elemental storage and excellent stability, which has been particularly appealing as a new kind of light absorbing material in high-performance solar cells [1–3], owing to its suitable bandgap (≈1.7 eV) and strong absorption coefficient (1.8×10^5 cm^{-1}). Meanwhile, it has a range of potential applications in photocatalysis [4] and energy storage [5]. Up to date, Sb_2S_3 1-D materials including nanorods [6,7], nanoribbons [8–10] and nanotubes [11,12] have been successfully synthesized. Pursuing convenient method to fabricate 1-D nanostructure with controllable size and shape is an interesting research work for the wider application fields. A solution-phase method for preparing Sb_2S_3 1-D materials, which is considered to be more promising, with the advantages of low cost and easy fabrication, was seldom reported in the past few years [13–15]. For example, Chen *et al* [16] obtained complex Sb_2S_3 hierarchical nanostructure by a hydrothermal reaction at 180°C for 12 h, with the assistance of polyvinyl pyrrolidone (PVP). Wu *et al* [17] fabricated the double cauliflower-like Sb_2S_3 by using hydrothermal method for a much longer time of 30 h. So these reported methods usually require the longer reaction time to complete the crystallization process.

Herein, high-purity Sb_2S_3 sheaf composed of nanorods (1.2–1.6 μm in length and 112 nm in width) is reported to be produced by using a simple hot-injection synthesis with several minutes. The uniformity in morphology and the copiousness in quantity suggest an ideal growth environment for the fabrication of crystalline Sb_2S_3 with this method. The formation mechanism for the growth process was also investigated in this work. It could be proved that the present strategy is an effective route to facilitate the nucleation-growth process and manipulate the microstructure of nanomaterials.

2. Experimental

Antimony trichloride ($SbCl_3$, 99.9%), 1-octadecene (ODE, 90%) and oleylamine (OAm, 80–90%) were purchased from Aladdin. Sulphur powder (S, 99.99%) was obtained from Sigma-Aldrich. All the materials were used directly without further purification.

In a typical process, 0.16 g sulphur powder was initially added into a 50 ml three-neck round-bottom flask containing 5 ml of OAm, followed by degassing with a flow of nitrogen. The solution was heated and stirred magnetically at 90° until the sulphur powder was completely dissolved. Then, 0.0456 g $SbCl_3$ was dissolved in 3 ml of OAm and 2 ml of ODE. The antimony precursor solution was heated up to a higher temperature (in the range of 180–210°C), under nitrogen flow and strong magnetic stirring. Then the as-prepared sulphur precursor solution was injected into the reaction system and remained for 5–20 min. Finally, the precipitation was collected through centrifugation.

The crystalline structure was measured by X-ray diffraction (XRD, BRUKER D8 ADVANCE) using Cu radiation

operated at 40 kV and 40 mA. The morphologies and compositions were obtained by using scanning electron microscope (SEM, FEI Nova Nano SEM450) and the energy-dispersive X-ray (EDX) spectroscopy, respectively. The high-resolution transmission electron microscope (HRTEM) and the corresponding selected-area electron diffraction (SAED) were performed with a PHILIPS CM200 microscope operating at 200 kV accelerating voltage. X-ray photoelectron spectroscopy (XPS) was measured by Thermo SCIENTIFIC ESCALAB 250Xi X-ray photoelectron spectrometer with Al Kα radiation (1486.6 eV). Raman spectrum analysis was performed on a HR Evolution Raman spectrometer, using an Ar-ion laser excitation with a wavelength of 532 nm. Absorption spectrum was recorded using a UV–Visible spectrophoto meter (Perkin Elmer Lambda 950).

3. Results and discussion

The XRD patterns of Sb_2S_3 samples synthesized at different temperatures are shown in figure 1a. When the hot-injection is performed at 180°C for 5 min, no obvious diffraction peaks of the sample are found, indicating that the sample is essentially amorphous. Peaks become sharper as the temperature increases to 190°C, although the intensity and shape of the diffraction peaks reveal that the sample is still not well crystallized. With further elevating the temperature up to 210°C and increasing the reaction time up to 20 min, the peak intensities steadily become stronger, demonstrating an enhancement of the crystallization. All the clear peaks can be well indexed to the orthorhombic phase of stibnite Sb_2S_3 (cell constants: $a = 11.24$ Å, $b = 11.31$ Å, $c = 3.84$ Å; JCPDS 42-1393). No characteristic peaks corresponding to impurities are detected, indicating that the as-prepared samples possess a highly pure phase. Raman spectrum was also performed to further investigate the formation of crystalline Sb_2S_3, as shown in figure 1b. For the sample synthesized at 180°C, the broad single peak at 293 cm^{-1} owing to the symmetric vibrations of SbS_3 pyramid [12,18] implies the weak crystallization. Then the peak is found to be splitted into two peaks at 280 and 305 cm^{-1}, which become much clearer as the temperature increases up to 210°C, suggesting the enhanced crystallinity of stibnite Sb_2S_3 [1,19]. These results are in accordance with the XRD.

Figure 2a–c shows the typical XPS of Sb_2S_3 synthesized at 210°C. The survey spectrum confirms the presence of Sb and sulphur elements. The two peaks at 529.12 and 538.56 eV can be assigned to Sb $3d_{5/2}$ and Sb $3d_{3/2}$, respectively. The peak at 161.21 eV is assigned to the binding energy of S $2p_{3/2}$. The results are consistent with the reported values in the literature [20]. The weak intensity of S $2p_{1/2}$ signal in 162.31 eV could be ascribed to a small amount of oxidation state of sulphur [21].

The morphology and structure of the products were also examined using TEM and SAED. When the reaction temperature is set at 180°C, the amorphous orange-red particles with the irregular shape in sizes ranging from 60 to 80 nm are immediately formed (figure 3a). It is worthwhile to note here that some adjacent nanoparticles join with each other, forming the connected clusters, as indicated by the dotted oval in the image. In figure 3b, it could be found that the small disordered bundles of nanorods are produced at 190°C for 5 min. Moreover, the obtained sample still consists of a large amount of amorphous nanoparticles and a small amount of short nanorods, ascribed to the incomplete reaction. As shown in the inset of figure 3b, the ambiguous lattice fringes demonstrate the poor crystallinity for this sample as well. It is inferred that the formation of bundle is probably due to the growth of each particle seed in the cluster. At 200°C, the longer bundles with simple splitting are formed (figure 3c).

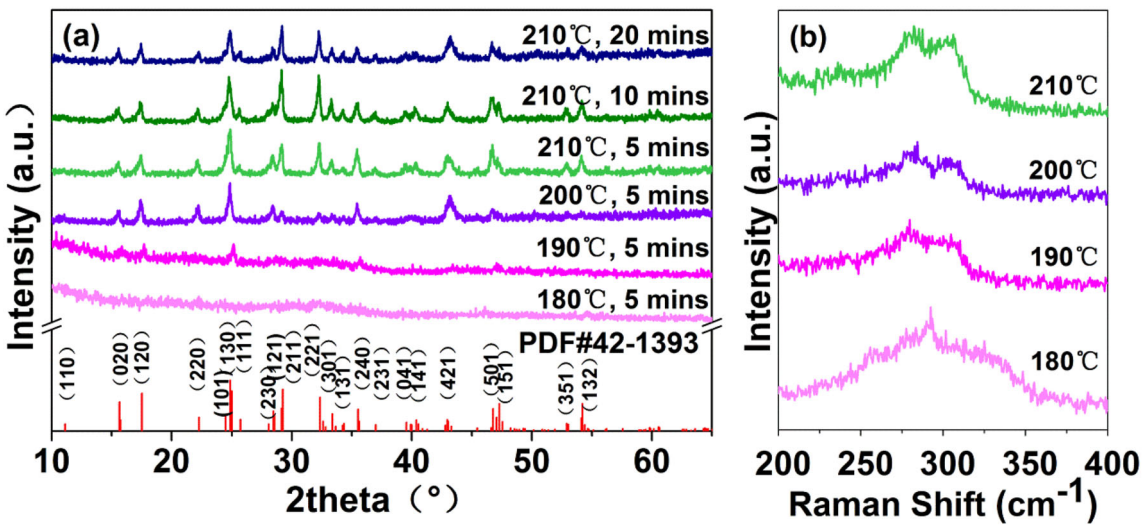

Figure 1. (**a**) XRD patterns and (**b**) Raman spectra of Sb_2S_3 nanorods synthesized at different temperatures and times.

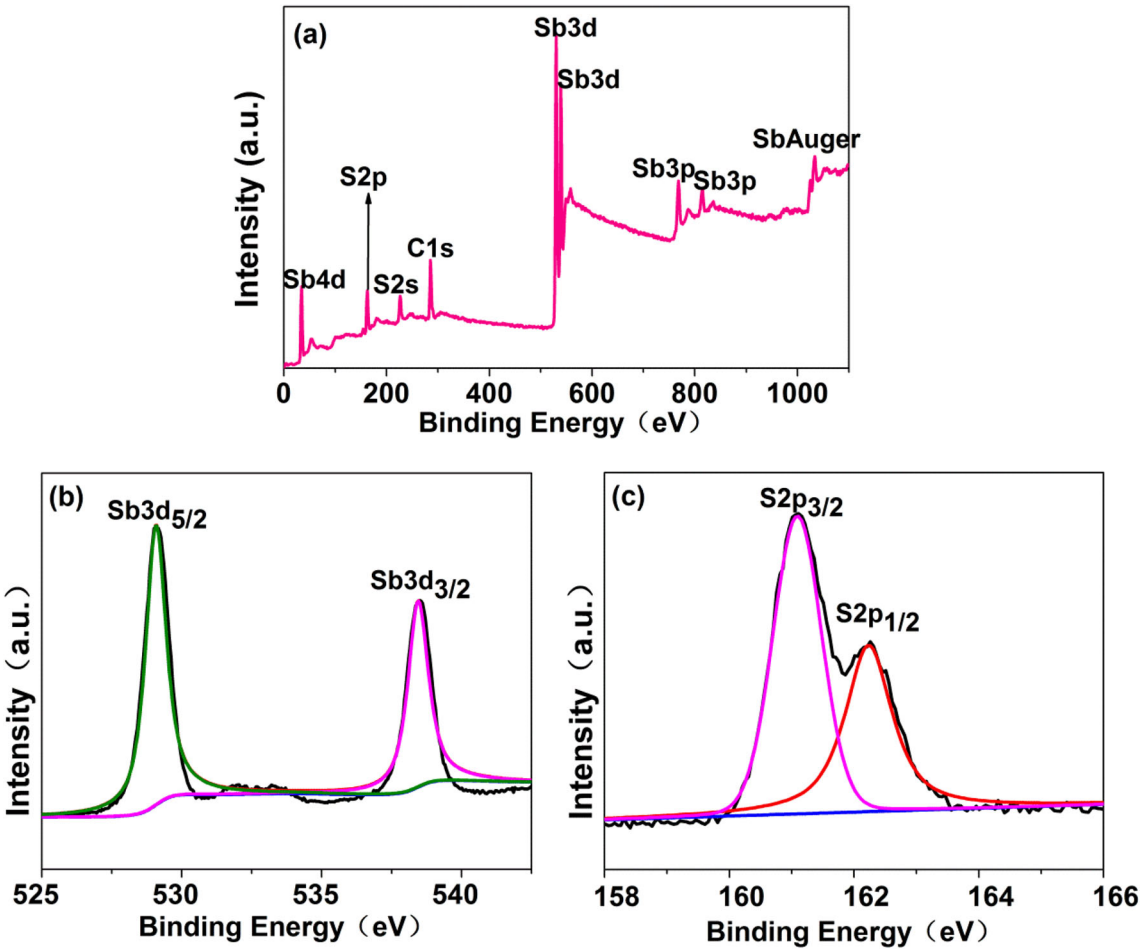

Figure 2. A typical XPS of Sb_2S_3 synthesized at 210°C for 5 min: (**a**) survey spectrum, (**b**) Sb3d and (**c**) S2p.

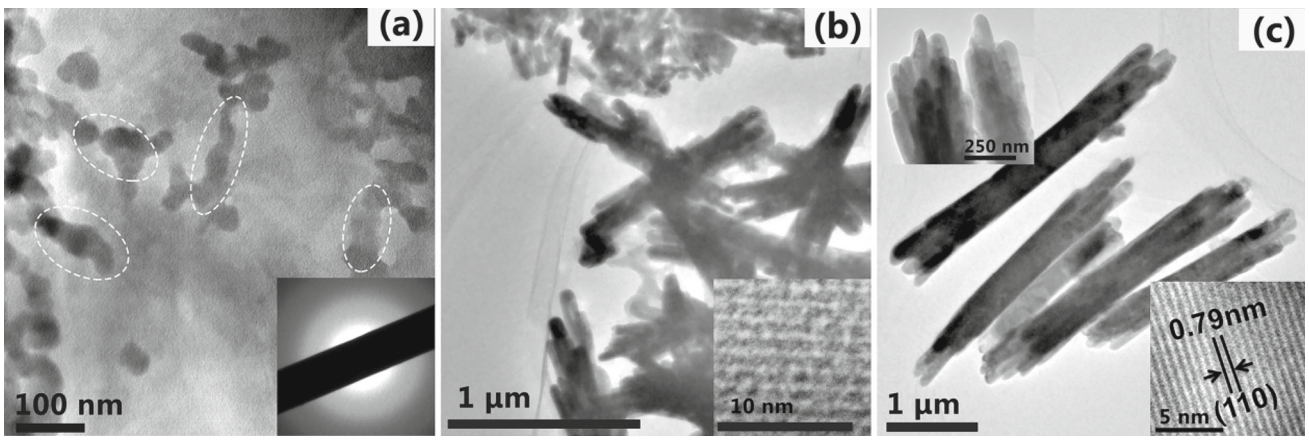

Figure 3. TEM images of Sb_2S_3 synthesized at 180–200°C for 5 min: (**a**) 180, (**b**) 190 and (**c**) 200°C; the inset in (**a**) is the corresponding SAED pattern; the insets in (**b**) and (**c**) are the corresponding HRTEM images, respectively.

The fringe spacing of 0.79 nm closely matches the interplanar spacing of the (110) plane of the orthorhombic phase of Sb_2S_3.

In order to further evaluate the influence of reaction time on the morphology of product in hot-injection synthesis, figure 4 presents TEM images of the sample synthesized at 210°C

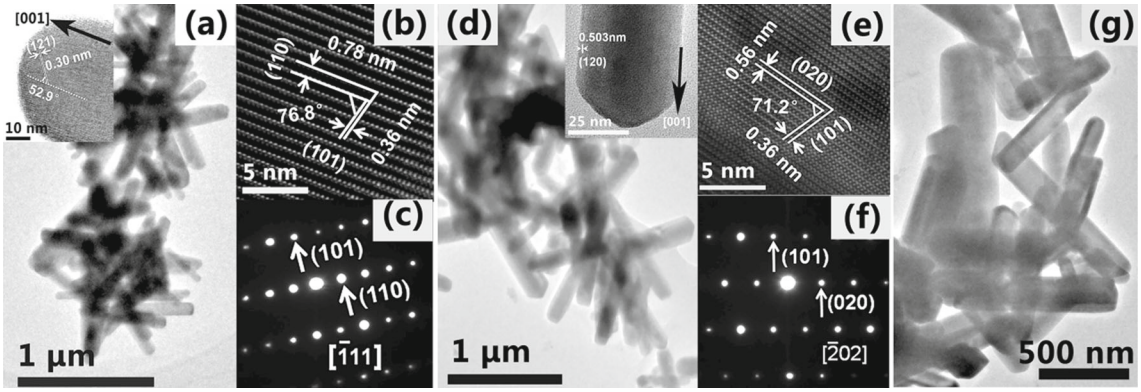

Figure 4. TEM images, HRTEM images and SAED patterns of Sb_2S_3 nanorods synthesized at 210°C for different reaction times: (**a**–**c**) 5, (**d**–**f**) 10 and (**g**) 20 min.

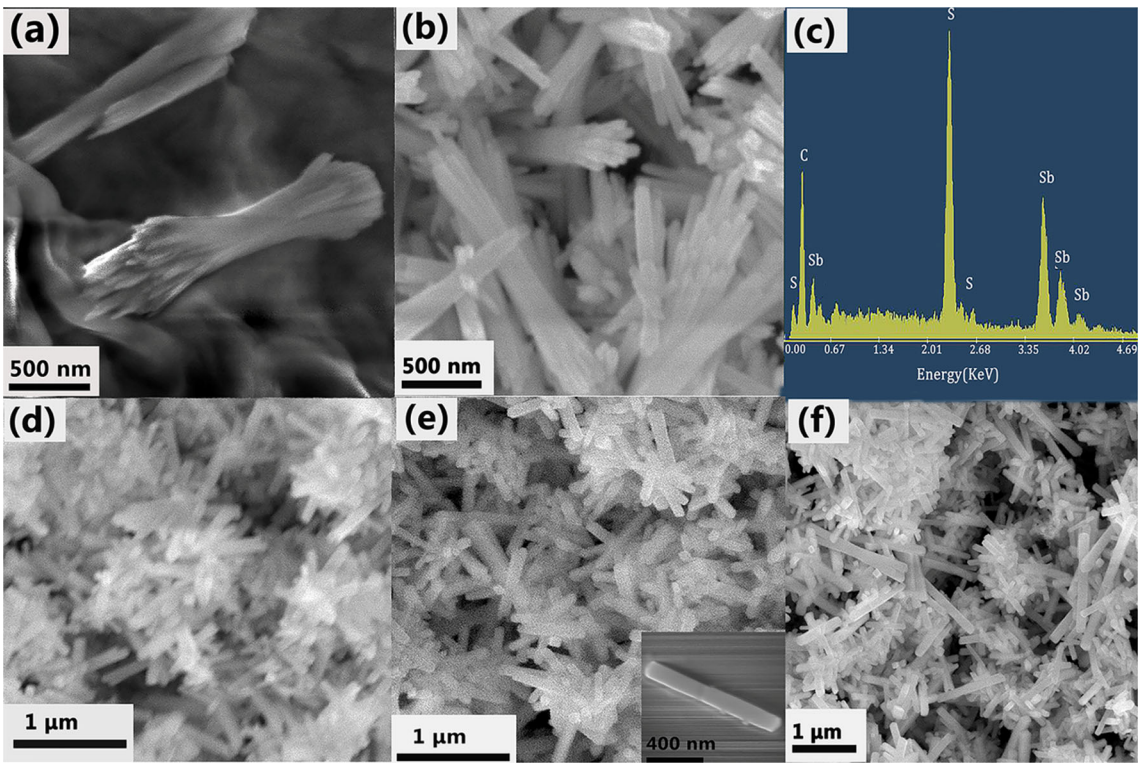

Figure 5. SEM images of samples synthesized at (**a**) 190 and (**b**) 200°C; (**c**) EDX spectrum corresponding to (**b**); SEM images of samples synthesized at 210°C for (**d**) 5, (**e**) 10 and (**f**) 20 min.

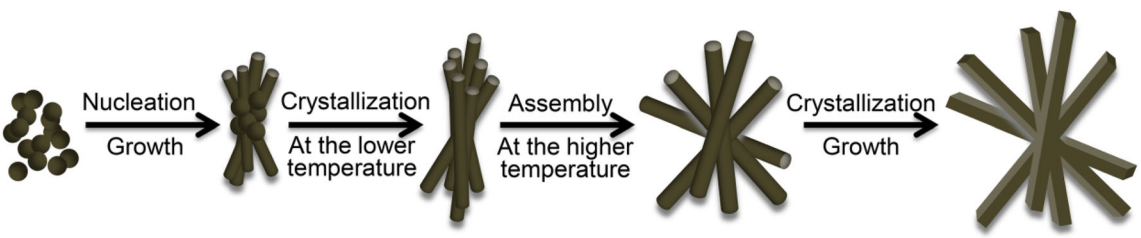

Figure 6. Schematic of growth mechanism for the as-prepared Sb_2S_3 with different morphologies.

for 5–20 min. In figure 4a, it clearly indicates that a lot of rod bundles appear as a sheaf of nanorods cross-linked in the middle, forming a sheaf-like microstructure. In the inset of figure 4a, the lattice spacing is about 0.30 nm corresponding to the (121) plane of a stibnite Sb_2S_3 structure. The angle between the (121) plane and growth direction is 52.9°, and thus it can be inferred that the nanorod grows along the *c*-axis, i.e., [001] direction. Figure 4b and c are the HRTEM image and SAED pattern, corresponding to an isolated nanorod, taken from the sample presented in figure 4a. As expected, both the lattice spacing and the SAED pattern can be assigned to the orthorhombic phase of Sb_2S_3, which could be evidenced by the literature with the similar reported data for Sb_2Se_3 nanoribbon [10]. Figure 4d shows a TEM image of Sb_2S_3 sample synthesized at 210°C for 10 min, where the inset is a corresponding HRTEM of an individual nanorod. A careful inspection indicates that the crystalline Sb_2S_3 sheaf structure is made up of a lot of closely packed and well-defined prismatic nanorods with uniform widths (112 nm) and lengths (1.2–1.4 μm). The discernible lattice fringes could reveal that the high-quality Sb_2S_3 product is obtained, without lattice defects (e.g., dislocation). Figure 4e indicates that the lattice spacings of 0.56 and 0.36 nm in the individual nanorod match well with the interplanar spacing of the (020) and (101) planes of stibnite Sb_2S_3, respectively, and the angle of 71.2° is in good agreement with the theoretical value. The corresponding SAED pattern (figure 4f) taken from [$\bar{2}$02] zone axis provides a further evidence to support an orthorhombic-structured Sb_2S_3. The length of nanorods becomes much longer (1.6 μm), while the reaction time increases up to 20 min, as shown in figure 4g.

Figure 5a presents the SEM image of Sb_2S_3 sample fabricated at 190°C for 5 min, clearly demonstrating that it exhibits rough morphology, except for very few bundles. The compact bundles of nanorods with uniform lengths (1.1 μm) and diameters (80 nm) are clearly observed for Sb_2S_3 product prepared at a higher temperature of 200°C (figure 5b). Both Sb and sulphur elements are observed in the EDX spectrum, as shown in figure 5c. The atom ratio of Sb:sulphur is 1:1.45, close to 2:3, suggesting an appropriate chemical composition of Sb_2S_3 in the nanorods. Further increasing the reaction temperature to 210°C, a large quantity of sheaf composed of uniform and slippery Sb_2S_3 nanorods can be observed, as illustrated in figure 5d. Prolonging the time subsequently could greatly reduce the amorphous phase, yielding well-crystallized and much longer nanorods with rectangular cross-section (figure 5e and f). The phenomenon is generally in agreement with that observed in TEM.

Here, we propose a possible formation mechanism for the growth process of Sb_2S_3, as described in figure 6. At the beginning of reaction, amorphous Sb_2S_3 nanoparticles are formed quickly. The collision of adjacent nanoparticles could result in the formation of agglomerated cluster while the dissolution and nucleation are going on. With the increase in temperature, the growth of each nanoparticle along the oriented *c*-axis direction produces the nanorod. Therefore, these primary nanorods tend to form the bundle-like structure. Further increasing the temperature up to a much higher temperature, higher energy will be involved in the reaction, inducing a self-assembly formation of sheaf-like structure made up of several nanorods with round cross-section. Subsequently, it could develop into the longer prismatic nanorods with rectangular cross-section, with prolonging the reaction time, due to the enhancement of crystallinity. In general, the uniformity in morphology and the copiousness in quantity of the crystalline Sb_2S_3 product fabricated by using the present hot-injection approach, imply an ideal growth environment in the reaction system. Furthermore, UV–Vis absorption spectra in figure 7 demonstrate a red shift of the absorption onset ranging from 722 to 783 nm. Thus, the bandgap value (1.58–1.72 eV) of the as-prepared Sb_2S_3 is close to its optimum value for photovoltaic application, which is the focus in our forthcoming work.

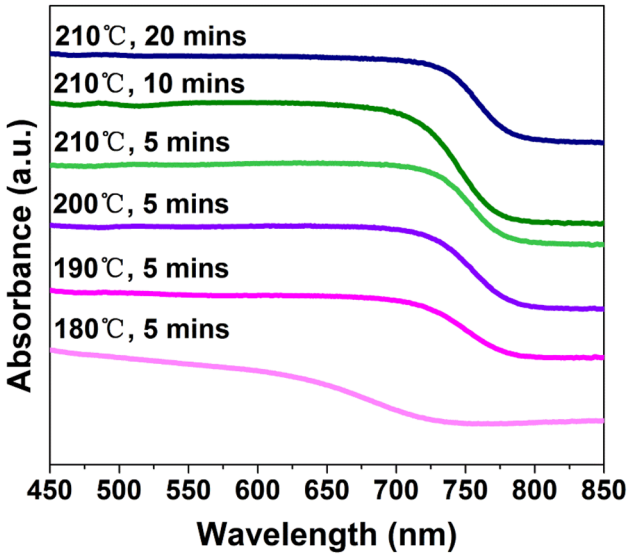

Figure 7. UV–Vis absorption spectra of Sb_2S_3 products.

4. Conclusions

In the present work, we succeeded in synthesizing high-quality Sb_2S_3 1-D material using a hot-injection method. The composition and purity of the as-prepared Sb_2S_3 sample were examined by XRD, Raman spectrum and XPS analysis. All the results reveal that the well-crystallized stibnite Sb_2S_3 with orthorhombic phase and high purity could be formed under the proper reaction conditions. The optical bandgap is calculated to be 1.58–1.72 eV. Under certain hot-injection condition, the evolution from amorphous Sb_2S_3 nanoparticles to a sheaf of Sb_2S_3 nanorods occurs with the increase in reaction temperature and time. At early stage of the nucleation process, the

agglomerated cluster of Sb_2S_3 amorphous particles can be formed *via* the collision among the adjacent nanoparticles. Then, the growth of each nanoparticle along the oriented *c*-axis direction produces the nanorod. These Sb_2S_3 nanorods develop into a bundle structure made up of nanorods with the round cross-section and the length of $\sim$1.1 μm, in subsequent growth stages, and complete their development as a sheaf of longer prismatic nanorods (1.2–1.4 μm in length), owing to the enhanced crystallinity. It would be expected to extend this reaction system for growing the other high-quality nanocrystals with novel morphologies.

Acknowledgements

This research was supported by the National Natural Science Foundation of China (No. 11604072). We wish to thank Hebei Key Laboratory of Opticelectric Information and Materials, and National and Local Joint Engineering Laboratory of New Energy Photoelectric Devices for the measurements assistance.

References

[1] Avilez Garcia R G, Meza Avendaño C A, Pal M, Paraguay Delgado F and Mathews N R 2016 *Mater. Sci. Semicon. Proc.* **44** 91
[2] Tang R, Wang X, Jiang C, Li S, Jiang G, Yang S *et al* 2018 *J. Mater. Chem.* **6** 16322
[3] Chauhan K, Deshpande M P, Patel K N, Chaki S H and Pandya S 2018 *Mater. Res. Express.* **5** 105005
[4] Zhang H, Hu C, Yong D and Yuan L 2015 *J. Alloys Compd.* **625** 90
[5] Xu Y, Chen W, Hu L, Pan X, Yang S, Shen Q *et al* 2019 *J. Alloys Compd.* **784** 947
[6] Zhang Z, Zhao J, Xu M, Wang H, Gong Y and Xu J 2018 *Nanotechnol.* **29** 335401
[7] Hou H, Jing M, Huang Z, Yang Y, Yan Z, Chen J *et al* 2015 *ACS Appl. Mater. Inter.* **7** 19362
[8] Caruso F, Filip M R and Giustino F 2015 *Phys. Rev. B* **92** 125
[9] Li S, Zhang Y, Tang R, Wang X, Zhang T, Jiang G *et al* 2018 *ChemSusChem* **11** 3208
[10] Yu Y, Wang R H and Chen Q 2006 *J. Phys. Chem. B* **110** 13415
[11] Bera S, Roy A, Guria A K, Mitra S and Pradhan N 2019 *J. Phys. Chem.* **10** 024
[12] Shuai X and Shen W 2012 *Nanoscale Res. Lett.* **7** 199
[13] Yang B, Xue D J, Leng M, Zhong J, Wang L, Song H *et al* 2015 *Sci. Rep.* **5** 10978
[14] Liu J 2014 *J. Synth. Cryst.* **43** 3318
[15] Gomis O, Vilaplana R, Manjon F J, Perez-Gonzalez E and Ursaki V V 2012 *J. Appl. Phys.* **111** 013518
[16] Chen G Y, Dneg B, Cai G B, Zhang T K, Dong W F, Zhang W X *et al* 2008 *J. Phys. Chem.* **112** 672
[17] Wu L, Xu H, Han Q and Wang X 2013 *J. Alloys Compd.* **572** 56
[18] Chen L, Zhu W, Han Q, Yang X, Lu L and Wang X 2009 *Mater. Lett.* **63** 1258
[19] An C, Tang K, Yang Q and Qian Y 2003 *Inorg. Chem.* **42** 8081
[20] Li C, Yang X, Liu Y, Zhao Z and Qian Y 2003 *J. Cryst. Growth* **255** 342
[21] Xu Y, Ye Q, Chen W, Pan X, Hu L, Yang S *et al* 2017 *J. Mater. Sci.* **53** 2016